KSCE Journal of Civil Engineering (2020) 24(4):1103-1115
DOI 10.1007/s12205-020-1540-x

pISSN 1226-7988, eISSN 1976-3808
www.springer.com/12205

Geotechnical Engineering

Physical Model Experiment of Surrounding Rock Failure Mechanism for the Roadway under Deviatoric Pressure form Mining Disturbance

Maolin Tian[a], **Lijun Han**[a], **Qingbin Meng**[a], **Chao Ma**[a], **Yijiang Zong**[a], **and Peiquan Mao**[a]

[a]*State Key Laboratory for Geomechanics and Deep Underground Engineering, China University of Mining and Technology, Xuzhou 221116, China*

ARTICLE HISTORY

Received 28 August 2019
Accepted 28 January 2020
Published Online 9 March 2020

KEYWORDS

Roadway deviatoric pressure
Mining disturbance
Physical model experiment
Deviatoric pressure stress field
Deformation failure mechanism

ABSTRACT

A physical model experiment was conducted to study the surrounding rock failure mechanism for the roadway under deviatoric pressure from mining disturbance. During the excavation process, a self-developed deviatoric pressure reaction system was used to realize deviatoric pressure loading. Meanwhile, a digital photogrammetric measurement system and a static strain data collection system were utilized to obtain the deformation, strain and stress of the model. The deviatoric pressure stress field characteristic and deformation failure mechanism of roadway were investigated by synthetic analysis of experimental data and displacement vector diagram. The physical experimental results showed that mining disturbance had an inevitable influence on the formation of roadway deviatoric pressure, which caused the V-shaped distribution of pressure stress above the roadway. The V-shaped deviatoric pressure stress caused the roadway asymmetric deformation that was proportional to the deviatoric pressure stress above the roadway. And the asymmetric deformation further aggravated the degree of deviatoric pressure stress and formed a vicious cycle, which resulted in the instability of the roadway. In addition, a numerical simulation under deviatoric pressure was conducted to verify the accuracy of physical experimental results. This study can provide helpful references for researching the instability behavior of the roadway.

1. Introduction

With increasing mining depth and continuous improvement of mining methods, the deformation failure mechanism of roadways under mining disturbance has become more complex. The mining influence and mine pressure tend to be serious due to the large mining height, large inclined length and large-scale fully mechanized caving (Yan et al., 2014). These easily cause serious deviatoric pressure on the roadway close to the working face, which results in serious local failure and asymmetric deformation failure of the roadway. Then, asymmetric deformation failure further aggravates the stress concentration and deviatoric pressure degree that make support difficult and seriously threatens the safety of coal mine production (Zhang and He, 2016). Hence, further understanding of the failure mechanism of roadway under deviatoric pressure from mining disturbance will help to reduce the problem and improve mining safety.

Nowadays, many studies involving the deformation failure and stability of roadways deformation have been carried out by using various methods including in-situ tests, laboratory experiments and numerical simulation (Sterpi and Cividini, 2004; Zhu et al., 2010, 2011; Zhang et al., 2016; Wang et al., 2017; Tian et al., 2019; Sun et al., 2019).

A physical model test in the laboratory is a common and effective method to analyze the deformation failure of geotechnical engineering. He et al. (2010a, 2010b) and He (2011) researched underground roadway excavation in geologically horizontal strata, 45° inclined rock, and vertical stratified rock with a physical model test based on infrared thermography. Sun et al. (2009) used numerical simulations to analyze the failure characteristics and coupling control countermeasures of the asymmetric deformation deep roadway within inclined rock strata. Then, Sun et al. (2017, 2018) performed physical modeling to investigate the deformation mechanism of tunnel with strata inclined ten degrees and tunnel with soft rock strata. Xiao et al. (2014) assessed the influence of buried depth and tectonic stress on

CORRESPONDENCE Lijun Han hanlj@cumt.edu.cn State Key Laboratory for Geomechanics and Deep Underground Engineering, China University of Mining and Technology, Xuzhou 221116, China

roadway deformation and stress by a physical model method. Yang et al. (2015) investigated failure modes of the jointed rock mass around the underground excavation by physical and numerical tests. Li et al. (2015) studied deformation mechanism of deeply buried roadways with a thick top coal by the model test method. Yang et al. (2018) reported a case of tunnel excavation with slanted upper-soft and lower-hard strata by physical and numerical tests, and discussed the failure mode of tunnel.

In addition, numerous researchers have developed numerical simulations to discuss the deformation and stability control of roadways (Coggan et al., 2012; Kang et al., 2014; Gao et al., 2015; Meng et al., 2016). Considering the high overburden and tectonic stress, Shen (2014) built a detailed numerical model by Universal Distinct Element Code (UDEC) to analyze the stability and deformation of soft rock roadways. Yan et al. (2014) proposed a new support system based on theory and numerical simulation, and this support system had been proven by field tests to have good control of large deformation. Fu et al. (2015) researched the displacement and rock bolt force of an underground cavern group in the reinforcement process by the modified discontinuous deformation analysis method.

Previous studies focused on the failure mechanisms of roadways, especially roadways under complex geological structures or special strata. However, there are few physical model experiments be conducted to investigate the surrounding rock failure mechanism of roadways under deviatoric pressure from mining disturbance. In this paper, in order to get a better understanding of the stress distribution and failure mechanism of deviatoric pressure roadways disturbed by an adjacent working face mining, we first carried out a large-scale physical model test equipped with static strain and digital photogrammetric measurement systems. The types of deviatoric pressure and the deformation failure of roadways under deviatoric pressure from mining disturbance can be obtained by analyzing the experimental results. Then, numerical models under deviatoric pressure were conducted to verify the result of the physical model.

2. Physical Model Experiment

2.1 Engineering Geological Condition

The deviatoric pressure roadway is located in the Yuncheng coal mining district, Shanxi province, China. The deviatoric pressure roadway, named the No. 20101 air return roadway, as shown in Fig. 1(a), was disturbed by the No. 20105 working face gob and the No. 20103 working face being mined, which led to local and asymmetric deformation failure in this roadway. The No. 20101 air return roadway was arranged along the No. 2 coal seam floor. The inclination angle of the strata is 2° – 4°, and the thickness of No. 2 coal seam is 6.2 m. The main exposed stratum lithology in the roof is sandy mudstone, siltstone and fine sandstone; meanwhile,

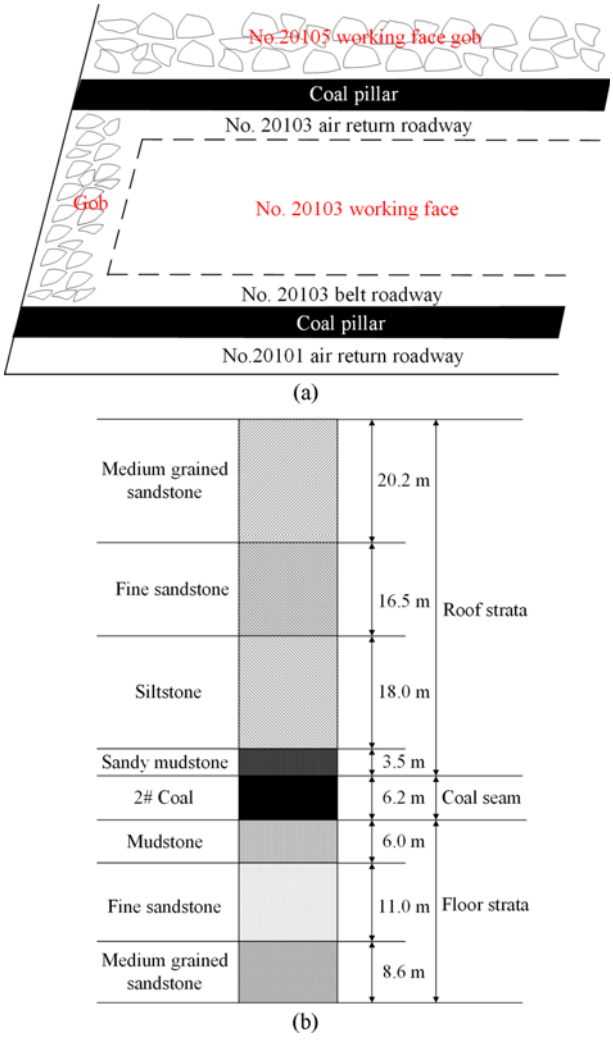

Fig. 1. The Location and Strata Histogram of the No. 20101 Air Return Roadway: (a) The Location of the No. 20101 Air Return Roadway, (b) Strata Histogram

Table 1. Physical and Mechanical Parameters of Roadway Surrounding Rock

Rock types	Density (kg/m^3)	Compressive strength (MPa)	Tensile strength (MPa)	Cohesive force (MPa)	Frictional angle (°)	Elastic modulus (GPa)	Poisson's ratio
Fine sandstone	2,645	58.5	2.98	8.36	45	23.99	0.31
Siltstone	2,651	63.5	2.67	9.48	32	19.48	0.19
Sandy mudstone	2,635	43.5	1.37	7.40	31	5.40	0.25
Coal	1,412	13.0	0.88	1.92	34	2.37	0.26
Mudstone	2,655	22.6	2.84	7.53	33	8.75	0.29
Medium grain sandstone	2,632	68.3	2.72	10.31	30	29.47	0.28

the main exposed stratum lithology in the floor is mudstone and medium grain sandstone, as shown in Fig. 1(b). Through the in-situ field coring and laboratory rock specimen physical and mechanical tests, physical and mechanical parameters of the real rock are obtained, as shown in Table 1.

2.2 Physical Experimental Design

2.2.1 Similarity Ratio and Similar Material

2.2.1.1 Similarity Ratio

The similarity principle is the theoretical foundation for physical model test, and geometry, boundary conditions, mechanical properties and initial stress conditions must satisfy the similarity principle. And similarity ratios are the ratios of real parameters to model parameters, which is important to reasonably carry out the physical model. According to the location of the deviatoric pressure roadway and the influence of overlying strata in the mining process, the strata of 90 m above and below the coal seam are taken as the modeling object to better reflect the influence of deviatoric pressure on the roadway. Then, combined with the laboratory equipment's dimension, the model can be established, the geometric similarity ratio C_l and bulk density similarity ratio C_γ of this physical model are determined to be 60 and 1.1, respectively. Other parameter similarity ratios can be obtained as follows:

$$C_\sigma = C_E = C_c = C_L \times C_\gamma = 66 \tag{1}$$

$$C_\mu = C_\varepsilon = C_\varphi = 1 \tag{2}$$

where C_σ is the similarity ratio of stress, C_E is the similarity ratio of elastic modulus, C_c is the similarity ratio of cohesion, C_μ is the similarity ratio of Poisson's ratio, C_ε is the similarity ratio of strain, and C_φ is the similarity ratio of the internal friction angle.

2.2.1.2 Similarity Material

Combined with the similarity principle and prototype parameters, river-sand was selected as aggregate, and calcium carbonate, gypsum and water were selected as cementing agents for similar materials. The density, compressive strength and elastic modulus which have great influence on the test results are selected as the key factors, the secondary parameters are negligible (Yang et al., 2018). The ideal similar materials parameters are listed in Table 2. By means of the principle of orthogonal design, 25 proportion schemes were designed to make 75 test specimens that were used in the mechanical experiments, as shown in Fig. 2. Then, the appropriate similar materials were selected to replace in-situ rock mass in the model by comparing the results of proportion schemes with the ideal parameter values, as shown in Fig. 3. The final selection result was listed in Table 3.

Table 2. Ideal Mechanical Parameters of Similar Materials

Rock types	Bulk density (kN/m^3)	Compressive strength (MPa)	Elastic modulus (GPa)
Fine sandstone	23.564	0.886	0.363
Siltstone	23.618	0.962	0.295
Sandy mudstone	23.476	0.659	0.082
Coal	12.579	0.197	0.036
Mudstone	23.653	0.342	0.133
Medium grain sandstone	23.448	1.035	0.447

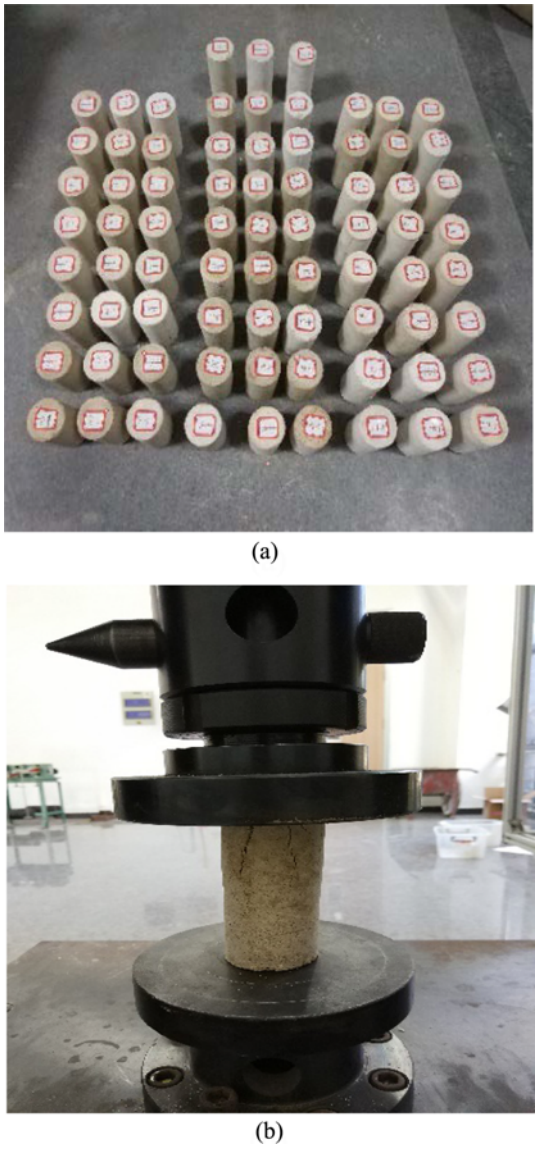

(a)

(b)

Fig. 2. Similar Material Specimens and Mechanical Experiments of Similar Material Specimens: (a) Similar Material Specimens, (b) Uniaxial Compression Test

2.2.2 Physical Model Test Equipment

A deviatoric pressure large-scale physical model test equipment, as shown in Figs. 4(a) and 4(b), is developed based on the KD-01 type plane stress simulator test frame. The equipment includes a hydraulic loading system, a reaction system, a constraint system and a monitoring system.

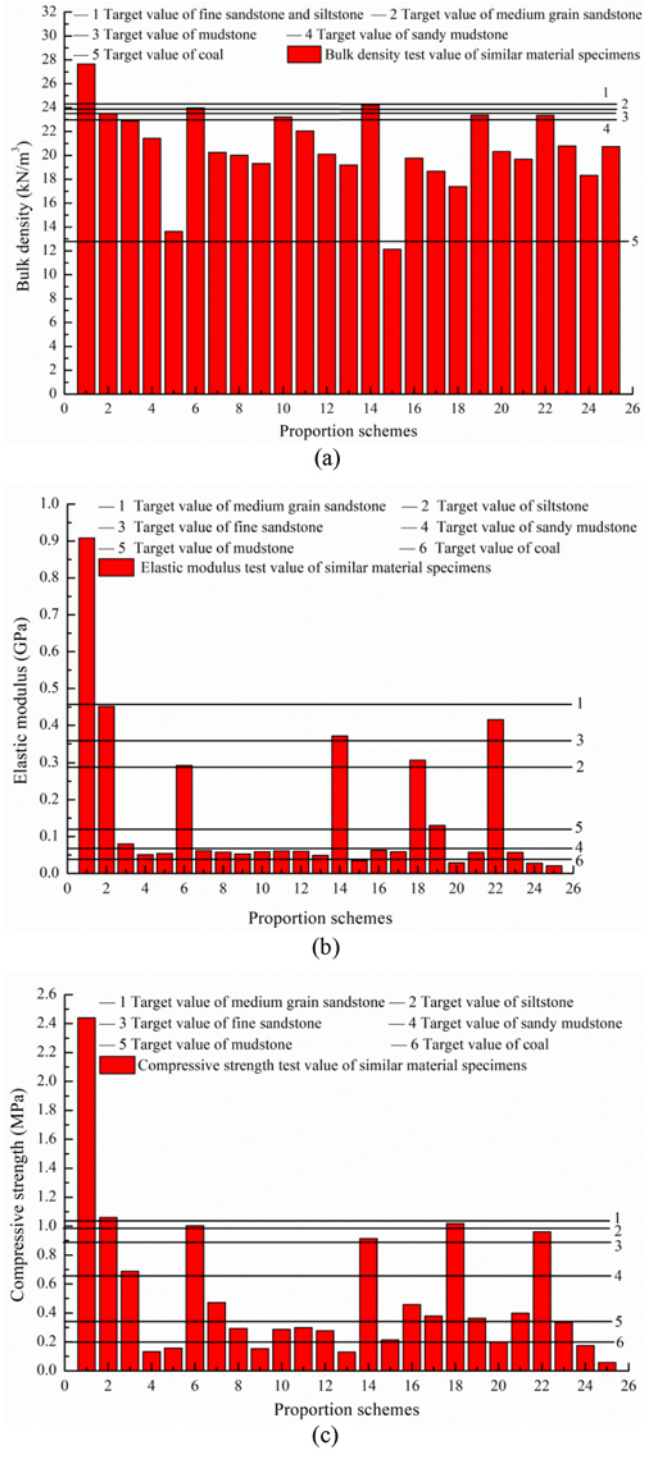

Fig. 3. Comparison of Similar Material Parameters and Target Values of In-situ Rock Parameters: (a) Bulk Density, (b) Compressive Strength, (c) Elastic Modulus

This type of plane stress simulator test frame can be used to conduct tests on models with dimension of 2,500 mm × 1,500 mm × 300 mm. This frame applies the load on the upper surface with 25 hydraulic jacks, but both sides of the frame are fixed constraints and cannot be loaded. The maximum output pressure of single hydraulic jack is 2 MPa, and it can maintain a constant load for a

Table 3. Selections of Similar Material Schemes

Rock types	Proportion schemes	(Calcium carbonate: Gypsum):River-sand:Water
Fine sandstone	14	(6:4):5:0.90
Siltstone	6	(7:3):5:1.35
Sandy mudstone	3	(6:4):5:1.05
Coal	15	(4:6):6:1.23
Mudstone	19	(6:4):7:1.00
Medium grain sandstone	2	(5:5):4:0.75

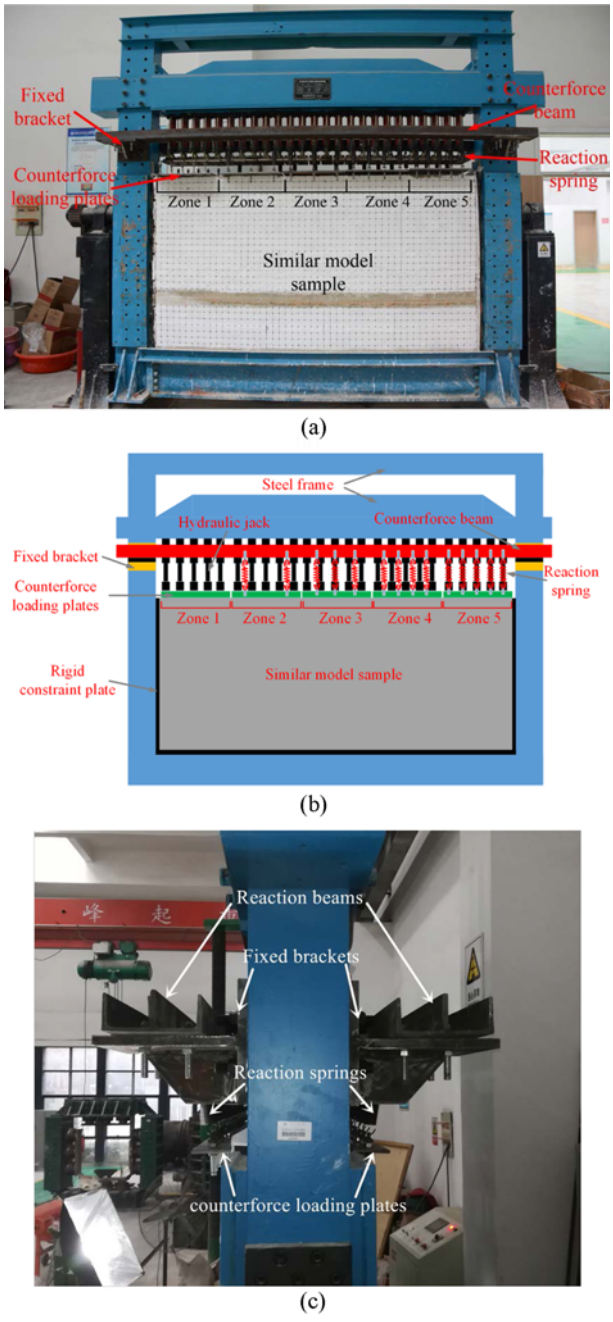

Fig. 4. The Deviatoric Pressure Large-Scale Geomechanical Model Test Equipment: (a) Photograph of the Geomechanical Model Test Equipment, (b) The Layout of the Experimental Equipment, (c) Side View of Self-Developed Deviatoric Pressure Reaction System

long time. Because the 25 hydraulic jacks are controlled by the same hydraulic control system, only a uniform load can be achieved. Thus, to apply deviatoric pressure on the upper surface, a deviatoric pressure reaction system is self-developed, as shown in Figs. 4(a) and 4(c). The principle of this self-developed deviatoric pressure reaction system is to use the spring deformation to form different tension on the 30 mm-thick loading plate to offset some of the pressure generated by the hydraulic jack. Then, the model can apply a deviatoric pressure gradient on the upper surface by hanging springs of different numbers in different zones, simulating the deviatoric pressure caused by the adjacent working face gob support pressure. The self-developed deviatoric pressure reaction system includes fixed brackets, counterforce beams, reaction springs and counterforce loading plates.

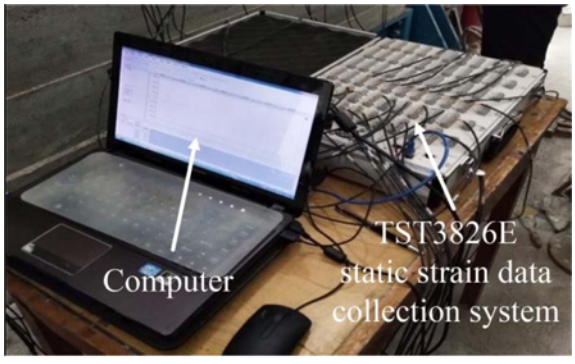

(a)

(b)

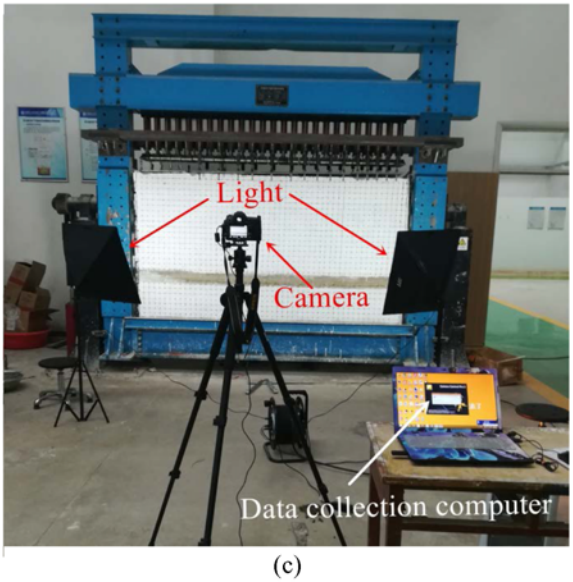

(c)

Fig. 5. Monitoring System: (a) TST3826E Static Strain Data Collection System, (b) SB-360 Strain-Type Miniature Pressure Boxes, (c) Digital Photogrammetric Measurement System

The monitoring system includes a static strain data collection system and a digital photogrammetric measurement system. The TST3826E (Taisite 3826E) static strain data collection system and the SB-360 strain type miniature pressure box, as shown in Figs. 5(a) and 5(b), are adopted to monitor the stress of surrounding rock, and they feature continuous measurement, high measurement accuracy, and fast, stable switching of monitoring points. SB-360 strain-type miniature pressure boxes are cylinders of 17 mm × 8.3 mm with small volume, which does not disturb the stress distribution in the model. The digital photogrammetric measurement system included a digital camera with 24,100,000 effective pixels, PhotoInfor software and the PostViewer post processor is used to measure the surface displacement of the model, as shown in Fig. 5(c). This system collects images with the camera and during the test process. Then, images are input to the PhotoInfor software and PostViewer post processor to obtain the displacement of the monitoring point by calculating the coordinate differences before and after deformation (Yang et al., 2018).

2.3 Physical Experimental Procedures

2.3.1 Model Construction and Layout of Monitoring Points

The model was built by filling and tamping similar materials according to the real rock strata, and thicknesses of strata from top to bottom are, respectively, 338 mm, 275 mm, 300 mm, 58 mm, 103 mm, 100 mm, 182 mm and 144 mm in the model, as shown in Fig. 6. Meanwhile, the pressure box was embedded in the position of a predesigned monitoring point in model construction. Monitoring section No. 1 was located 30 mm below the upper surface of the model, which facilitated the measurement of the initial deviatoric load value applied by the test system. Monitoring section No. 2 was located 80 mm above the coal seam. The monitoring points 9 – 23# with intervals of 100 mm were above the working face and coal pillar, and they intuitively reflected the stress state of the working face roof during the mining process. In addition, monitoring points 6 – 8# monitored the No.1 roadway roof and monitoring points 24 – 26# monitored the No.2 roadway roof, and they intuitively monitored the stress variation of roadway roofs during the mining process. Monitoring section No. 3 was located in the middle of the roadway, which is convenient for monitoring the stress variation trend of the two sides. Monitoring points 27# and 28# were 20 mm and 120 mm,

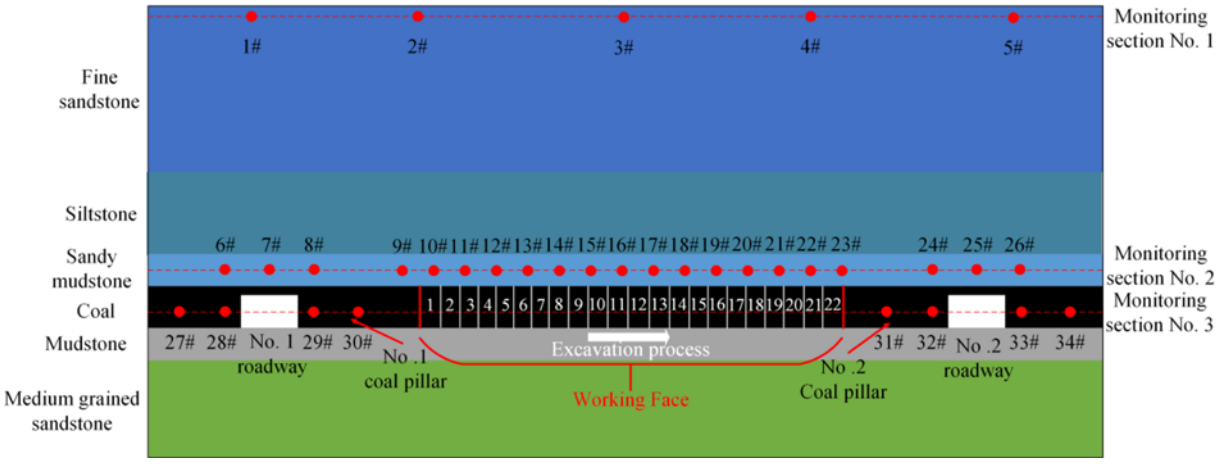

Fig. 6. Schematic Diagram of Monitoring Sections and Excavation Process

respectively, away from the left side of the No. 1 roadway, while monitoring points 29# and 30# were 20 mm and 120 mm, respectively, away from the right side of the No.1 roadway. Simultaneously, at the same depth from the two sides of the No. 2 roadway, monitoring points 31# and 32#, were embedded in the left side, while monitoring points 33# and 34# were embedded in the right side.

2.3.2 Initial Loading

Using engineering background, to simulate the deviatoric pressure caused by adjacent working face gob support pressure, the deviatoric pressure load applied on the upper surface of the model gradually increased from left to right. Because it is difficult to realize a linear deviatoric pressure load increase, the deviatoric pressure load is simplified to be applied as a step gradient increasing load. The 25 hydraulic jacks of the KD-01 model test frame were divided into five groups, which were divided into five zones in turn from left to right: I, II, III, IV and V. Thereafter, a deviatoric pressure load was realized by hanging 10, 8, 6, 4 and 0 reaction springs to provide different reaction forces between the loading plate and the reaction beam.

According to the field data and the similarity ratio of stress, the vertical loads applied in the upper surfaces of zones I – V are 0.4 MPa, 0.425 MPa, 0.45 MPa, 0.475 MPa and 0.5 MPa, respectively. Thus, the supply pressure of the hydraulic control system is 0.5 MPa, and the counterforce load generated by the spring counterforce group can be obtained according to the following equation:

$$F_i = (q - q_i)S \tag{3}$$

where F_i is the counterforce load value of each region, i = I, II, III, IV and V; S is the area of the counterforce loading plate, which is 0.1218 m^2; q is the supply pressure of the hydraulic control system; and q_i is the actual load value in each zone of the model.

The counterforce load values in each zone are shown in Table 4. Then, the deviatoric pressure load was realized by adjusting the deformation of the spring counterforce groups in each zone.

Table 4. The Deviatoric Pressure Load for Each Zone

Zone	Number of reaction springs	Actual load (MPa)	Counterforce load (MPa)	Counterforce of reaction springs (N)
I	10	0.400	0.100	12 180
II	8	0.425	0.075	9 135
III	6	0.450	0.050	6 090
IV	4	0.475	0.025	3 045
V	0	0.500	0	0

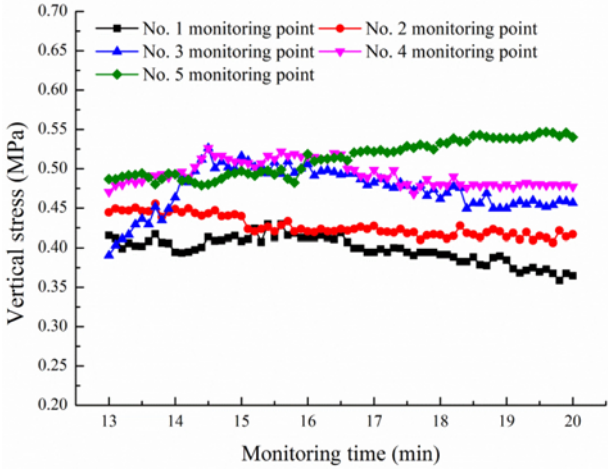

Fig. 7. Stress Variation at Monitoring Points of Monitoring Section No. 1

The hydraulic control system was turned on for loading, letting hydraulic jacks, reaction loading plate and model surface fully contact, and the load value tended to be stable for 20 minutes. The data of pressure boxes in monitoring section No. 1 are collected and sorted out, and the trend of stress variation for 13 – 20 minutes is drawn, as shown in Fig. 7. As shown in Fig. 6, the deviatoric pressure load of the model is gradually stabilized. The measured values of monitoring points 1# – 5# are 0.365

MPa, 0.436 MPa, 0.463 MPa, 0.479 MPa, and 0.535 MPa, respectively, which are 8.8%, 2.6%, 2.8%, 0.8%, and 7.0% higher than the theoretical values. The transmission error of the deviatoric pressure load is within the allowable range, which basically satisfies the test requirements.

2.3.3 Excavation

After applying the deviatoric pressure load, two rectangular roadways with a size of 95 mm × 60 mm that were 150 mm away from the edge of both sides of the model were excavated through artificial drilling. The mining length of coal seam is 1,500 mm, and the width of the coal pillars on both sides is 250 mm. The coal seam excavation was completed in 22 steps, and the single excavation length was 60 mm by artificial drilling. The excavation sequence of coal seam is shown in Fig. 6.

3. Physical Model Experiment Results Analysis

3.1 Analysis of Surrounding Rock Stress

With the advance of working face, the surrounding rock stress fields of the roadway and working face change constantly. The surrounding rock stress field in this model was analyzed based on monitoring pressure box data. Fig. 8 shows the vertical stress evolution of roadways and the working face roof for different mining distances, and Fig. 9 shows the vertical stress of different depths away from the two sides of roadways in different mining distances.

3.1.1 Stress Characteristics of Roadways and the Working Face Roof

Combining Fig. 8 and the monitoring point locations in Fig. 6, the conclusions of the analysis are:

1. Because the No.1 roadway is close to the initial mining position of the working face, it is always in a state of high deviatoric pressure stress. The high stress is concentrated on both sides of the roadway, whereas the stress value in the middle of the roadway roof is small, and has obvious asymmetry. Among them, due to stress release after excavation, stress transferred from the roof to both sides of the roadway. However, the limited bearing capacity of the coal pillar near the working face leads to serious deformation and destruction, which further deteriorates the mechanical properties of the coal pillar. This intensifies the transfer of stress to the entity coal side. Thus, the deviatoric pressure stress at monitoring point 6# is greater than at monitoring point 8#, and the distribution of deviatoric pressure stress above the roadway is V-shaped with "left highest-middle low-right higher". In addition, with the advancing working face, the increasing gob area results in the overburden strata pressure of the coal seam gradually transferring to the No. 1 coal pillar and the No. 1 roadway roof, which makes the deviatoric pressure stress continuously increase and aggravates the asymmetry degree.
2. With the advancing of working face, the vertical stress of monitoring points 9# and 23# that are above the No. 1 and No. 2 coal pillars, respectively, increases continuously. Because the No. 1 coal pillar is close to the initial mining face, the vertical stress of monitoring point 9# changes greatly in the early stage of mining, and then the growth rate of the vertical stress decreases gradually. In contrast, because monitoring point 23# is located in the stopping line pillar, its vertical stress is less affected by mining in the early

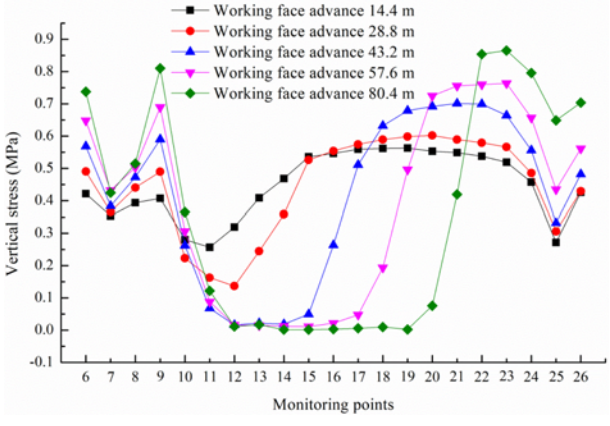

Fig. 8. Stress Variation at Monitoring Points of Monitoring Section No. 2

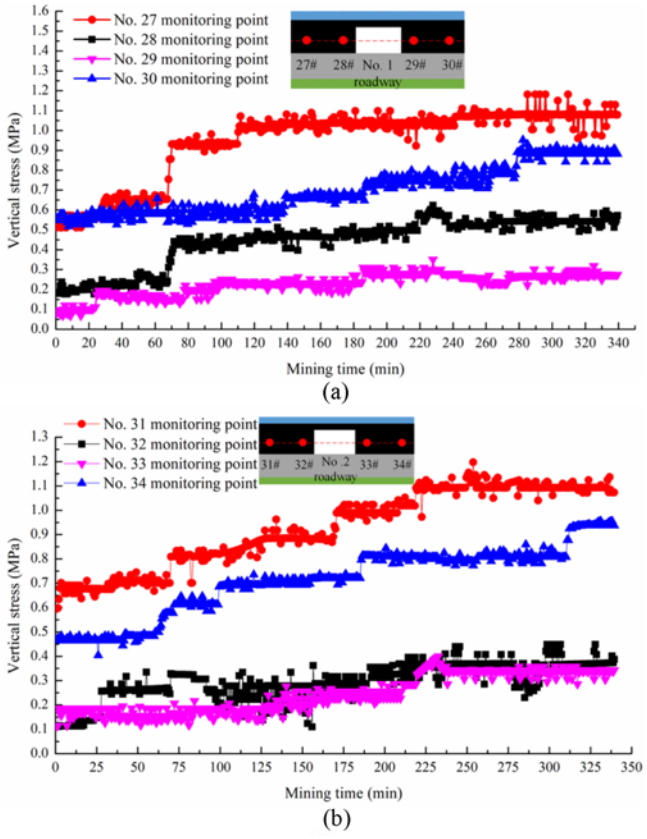

Fig. 9. Vertical Stress of Monitoring Points on the Two Sides of the Roadway: (a) Variation of Vertical Stress of the No. 1 Roadway, (b) Variation of Vertical Stress of the No. 2 Roadway

stage and remains original rock stress. However, the stress increases greatly when the working face advances to approximately 43.2 m and then the growth rate of the vertical stress increases gradually.

3. With the advancing of working face, the variation of vertical stress at monitoring points 10# – 22# located on the coal seam roof is consistent with the support pressure. When the working face advances to 43.2 m, part of the gob roof collapses, and the measured values of the pressure box at monitoring points 12# and 13# are approximately 0. The working face continues to advance, and the following pressure box monitoring points 14# – 19# also fall, and the measured valued tend to be 0.
4. Because the No.2 roadway is near the end mining face, the vertical stress states of monitoring points 24# – 26# are basically stable in the early stage of mining (working facing in 0 – 43.2 m). The deviatoric pressure state of the No. 2 roadway is mainly caused by stress transfer to two sides due to unloading from roadway excavation. Because the width of the left pillar of the No. 2 roadway is far larger than the right pillar, and the transferred stress results in serious deformation of the right coal pillar and reduces the bearing capacity, it leads to the stress further transferring to the left again. Thus, the V-shaped distribution characteristics of the "left high-middle low-right high" are formed. When the working face advances to 43.2 m, the vertical stress of monitoring points 24# – 26# increases sharply under the disturbance of mining. With the advancing of working face, the left coal pillar of the roadway becomes gradually narrower, and the increment of vertical stress increases continuously. The deformation of the left coal pillar of the roadway intensifies. When the working face advances to 80.4 m, the failure of coal pillars on both sides is similar, and the stress difference between monitoring points 24# and 26# decreases. However, the vertical stress value of monitoring point 24# is still higher than that of monitoring point 26# under the influence of support pressure, and shows the V-shaped distribution characteristics of "left highest-middle low-right higher".

3.1.2 Stress Characteristics of the Two Sides of the Roadway

Combining Fig. 9 and the monitoring point locations in Fig. 6, the conclusions are summarized as follows:

1. The No. 1 roadway is close to the first mining face location, and the vertical stress of both sides is greatly affected by mining in the early stage of mining, as shown in Fig. 9(a). The right coal pillar of the roadway is seriously broken, which results in a decline in bearing capacity and the vertical stress transferring to the left of the roadway. Hence, the right side stress is generally lower than the left side stress. The vertical stress increases slowly and steadily, and finally tends to be stable with the advancing of working face. When the working face advances to 43.2 m (excavation for 70 minutes), the left side vertical stress of the No. 1 roadway suddenly increases due to the roof movement of the gob. Thereafter, with the working face gradually away from the No. 1 roadway, the impact of mining on the No. 1 roadway is gradually diminishing, and the left side stress increases steadily and eventually tends to be stable.
2. The vertical stress of both sides of the No. 2 roadway is less affected by mining and basically remains stable in the early stage of mining, as shown in Fig. 9(b). Thereafter, with the advancing of working face, the stress at deep monitoring points on both sides increases stepwise synchronously. Because the left side is closer to the working face, the stress on the left side of the roadway is higher than on the right side, and the stress increment is greater than on the right side. The stress at shallow monitoring points on both sides increases with the approaching the working face. However, the variation of stress is small and gentle due to serious damage of the shallow surrounding rocks on the two sides and a significant reduction of bearing capacity.

3.2 Analysis of Surrounding Rock Displacement

The convergence law of rock around a roadway is reflected by the digital photogrammetric measurement system. Fig. 10 is the displacement vector diagram of the model under the initial deviatoric pressure load during the period from roadway excavation to the first mining of the working face. Figs. 11 and 12 are, respectively, the displacement diagram of the roadway surface and the displacement vector diagram of roadways surrounding rock in the mining process.

3.2.1 Displacement Characteristics of the Model under Initial Deviatoric Pressure Load

After the comparative analysis in Figs. 10 and 11, the conclusions of the analysis are:

1. The surface displacement of the model increases in turn from left to right under the initial deviatoric pressure load, and the maximum displacement appears at the upper right of the model. The angle between the displacement zoning boundary and the horizontal line is approximately 135°, and the displacement vector of the upper overburden rock points to the lower left.

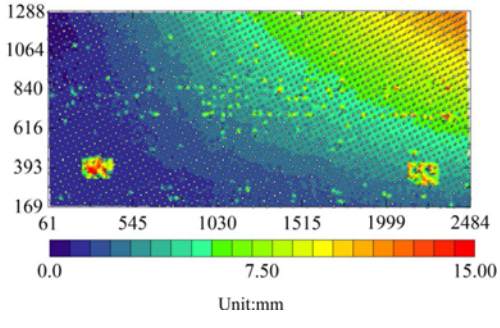

Fig. 10. Vector Diagram of Model Displacement under Initial Deviatoric Pressure Load

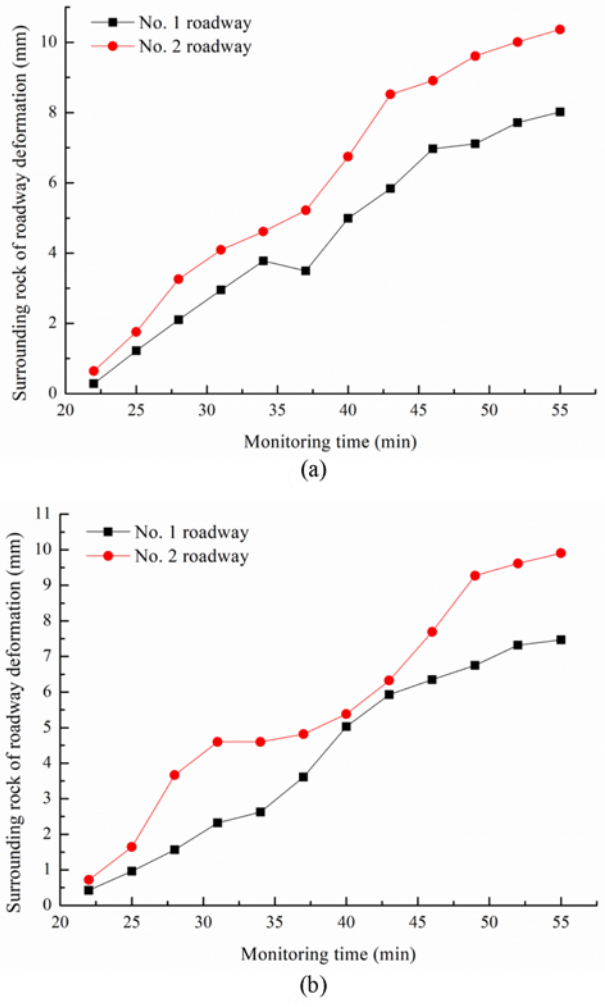

Fig. 11. Roadway Surface Displacement under Initial Deviatoric Pressure Load: (a) Roof to Floor Convergence, (b) Deformation of Two Sides

2. The deformation trend of roadway surrounding rock is generally consistent under a step gradient for increasing the initial deviatoric pressure load. After excavation, the stress of the surrounding rock can be released in a short time, and rock mass on the roadway surface changes from triaxial stress state to biaxial stress state. The surrounding rock deformation increases rapidly, and then the deformation rate decreases gradually and finally tends to be stable. However, because the No. 1 roadway is located in the low deviatoric pressure load area, the deformation of the No. 1 roadway is less than that of the No. 2 roadway.

3.2.2 Displacement Characteristics of Roadways under Deviatoric Pressure form Mining Disturbance

By analyzing Fig. 12, the conclusions are summarized as follows:

1. During the mining process, the No. 1 roadway shows asymmetric deformation. Under the deviatoric pressure stress caused by mining, the right side deformation is always greater than the left side, and the deformation and failure of the two sides are mainly concentrated in the upper and middle parts and gradually develops to the lower part. In addition, with the advance of working face, the deviatoric pressure stress of the right roof of the No. 1

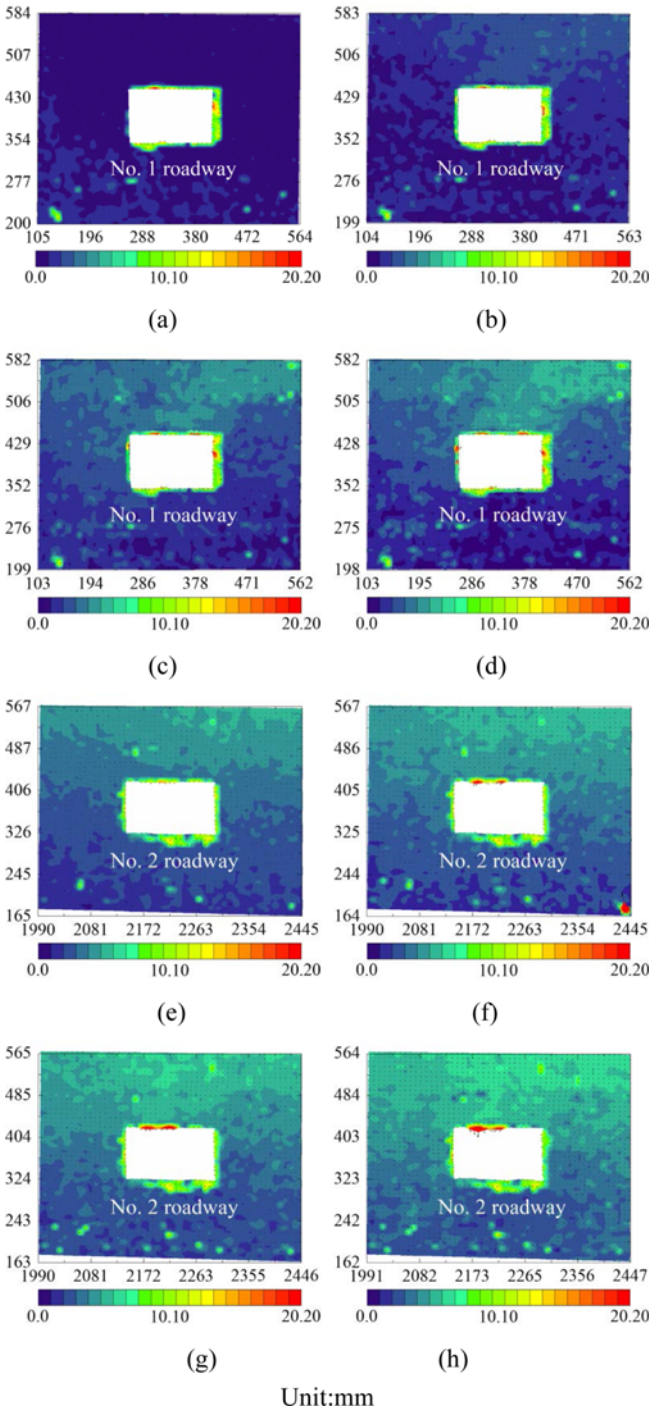

Fig. 12. Displacement Vector Diagram of Roadway Surrounding Rock under Mining Disturbance: (a) Mining to 28.8 m (No.1 Roadway), (b) Mining to 43.2 m (No.1 Roadway), (c) Mining to 57.6 m (No.1 Roadway), (d) Mining to 80.4 m (No.1 Roadway), (e) Mining to 28.8 m (No.2 Roadway), (f) Mining to 43.2 m (No.2 Roadway), (g) Mining to 57.6 m (No.2 Roadway), (h) Mining to 80.4 m (No.2 Roadway)

roadway continues to increase, which results in larger subsidence of the upper strata on the right side roof, and the right side roof subsidence is always greater than the left side.

2. Because the No. 2 roadway is near the end of the mining face, it is less affected by mining in the early stage of mining, and the asymmetric deformation of the roadway is not obvious. However, the left side roof subsidence of the roadway is obviously larger than the right side when the working face advances to approximately 43.2 m. The asymmetric deformation of the roof is aggravated with the advancing of working face. In addition, because the initial deviatoric pressure stress of the No. 2 roadway is greater than that of the No. 1 roadway and the deviatoric pressure stress is further increased under the disturbance of mining in the later stages, the surrounding rock displacement of the No. 2 roadway is larger than that of the No. 1 roadway.

4. Numerical Simulation

4.1 Numerical Model

In order to facilitate comparison with physical model test results, a numerical simulation that had the same dimensions, boundary conditions, excavation processes and mechanical parameters as the physical model was conducted. The dimensions of the numerical model are 2.5 m (width) × 1.5 m (height) × 0.3 m (thickness), as shown in Fig. 13. The three-dimensional numerical model contains 140,625 zones and 153,216 grid-points. Ten monitoring points around two roadways that are the same as that of physical model test are installed. In this simulation, the Mohr-Coulomb criterion is used and mechanical parameters of the rock mass are given in Table 5.

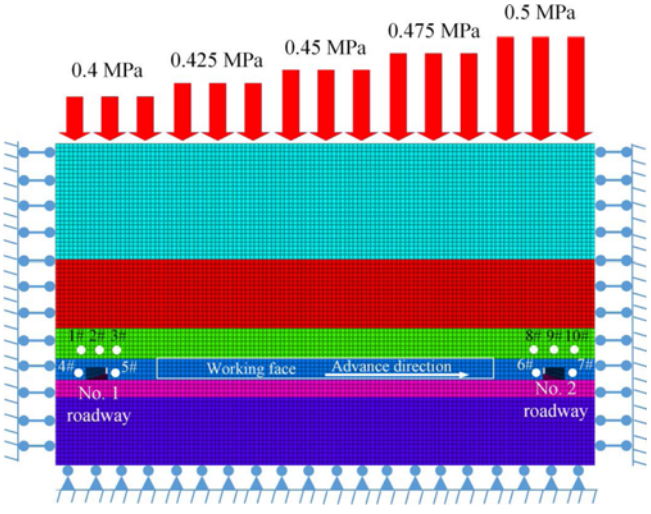

Fig. 13. Numerical Model

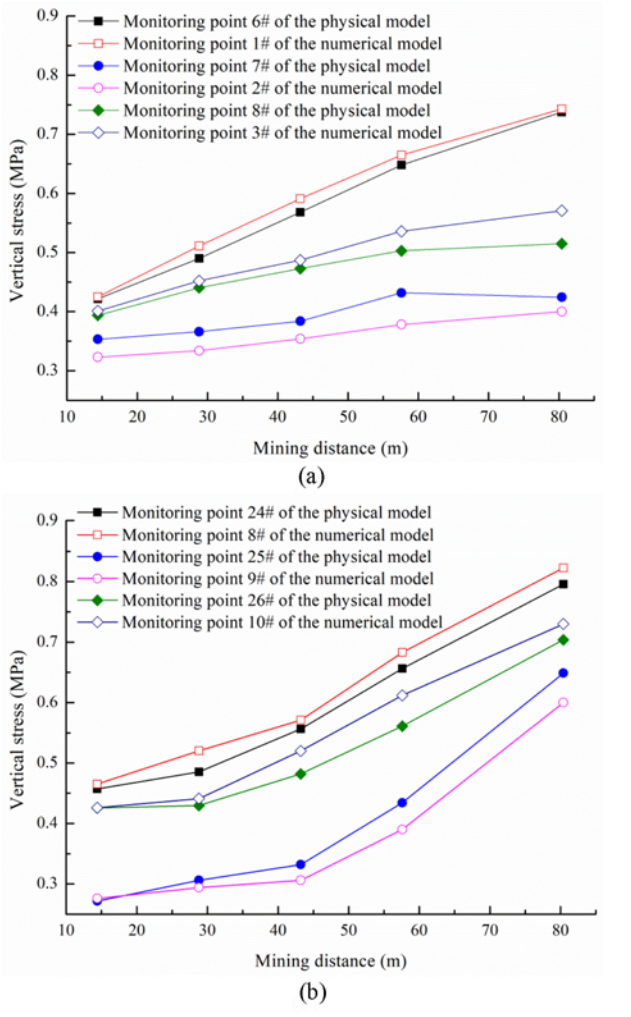

Fig. 14. Vertical Stress Comparison between Physical and Numerical Models: (a) Roof Monitoring Points of the No. 1 Roadway, (b) Roof Monitoring Points of the No. 2 Roadway

Table 5. Mechanical Parameters of Surrounding Rock for Numerical Simulation

Rock types	Density (kg/m^3)	Compressive strength (MPa)	Tensile strength (MPa)	Cohesive force (MPa)	Frictional angle (°)	Elastic modulus (GPa)	Poisson's ratio
Fine sandstone	2,404.5	0.886	0.045	0.127	45	0.363	0.31
Siltstone	2,410.0	0.962	0.040	0.144	32	0.295	0.19
Sandy mudstone	2,395.5	0.659	0.021	0.112	31	0.082	0.25
Coal	1,283.6	0.197	0.013	0.029	34	0.036	0.26
Mudstone	2,413.6	0.342	0.043	0.114	33	0.133	0.29
Medium grained sandstone	2,392.7	1.035	0.041	0.156	30	0.447	0.28

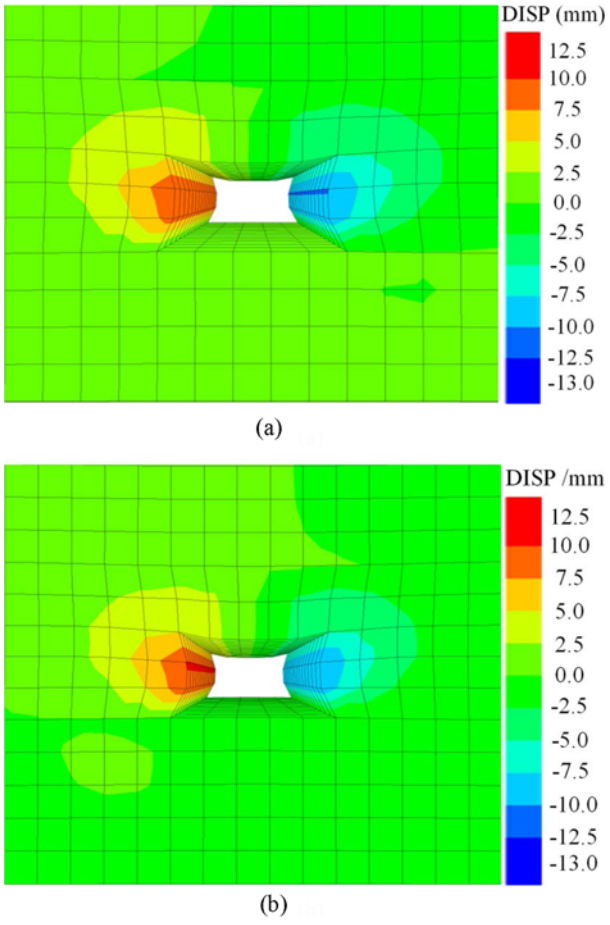

Fig. 15. The Displacement Field of Surrounding Rock after Excavation: (a) The Displacement Field of the No. 1 Roadway, (b) The Displacement Field of the No. 2 Roadway

4.2 Calculation Results

The vertical stress of monitoring points was obtained from the physical and numerical model results, as shown in Fig. 14, which was obtained that the vertical stress of roadway had a consistent variation trend in both models. However, the vertical stress on both sides of the roadway roof of the numerical model is larger than that of the physical model, and the vertical stress in the middle of the roadway is smaller than in the physical model. In this case, the material in the numerical simulation is more homogeneous than in the physical model, and the stress transfer is more sufficient in the numerical model. In the numerical simulation, the deviatoric pressure stress caused by mining results in the increase of vertical stress above the roadway, and the stress in the middle of the roadway can be more fully transferred to both sides of the roadway after the excavation. Thus, there are some discrepancies between the numerical and physical models.

The displacement field of the rock surrounding two roadways after excavation is shown in Fig. 15. It can be obtained from the result that the displacement of the two roadways is asymmetric. The right side displacement is greater than the left side displacement around the No. 1 roadway; however, the left side displacement is obviously larger than the right side displacement around the No. 2 roadway. The displacement of monitoring points 4# and 5# on both sides of the No. 1 roadway are 9.50 mm and 10.08 mm in the numerical model, respectively. The displacement of monitoring points 6# and 7# on both sides of the No. 2 roadway are 10.40 mm and 9.83 mm in the numerical model, respectively.

5. Discussions

This study focused on the influence of the adjacent working face mining on the stress distribution and deformation failure of the roadway based on the practical engineering. It is different from the previous research which focused on the influence of tectonic stress and special strata on the failure of roadway (Xiao et al., 2014; Sun et al., 2018). The physical model experiment nicely reflects the evolution law of stress field and displacement field of roadway under the deviatoric pressure though using the self-developed deviatoric pressure reaction system. The results of physical model experiment indicate that the deviatoric pressure stress above the roadway is V-shaped distribution under the influence of mining. The V-shaped deviatoric pressure stress causes the roadway asymmetric deformation, and the degree of asymmetric deformation is proportional to the deviatoric pressure stress above the roadway, which is similar to the large deformation of roadway caused by stress concentration (Shen, 2014; Yang et al., 2017). However, compared with the surrounding rock stress produced by the tectonic stress or the deep burial high stress, the deviatoric pressure stress from mining disturbance above the roadway is constantly variable. The degree of V-shaped deviatoric pressure of the roadway increases with the adjacent advancing working face. The increase of deviatoric pressure stress aggravates the asymmetric deformation, and the asymmetric deformation further aggravates the concentration degree of deviatoric pressure stress. Finally, they promote each other to form a vicious cycle, which seriously affected the stability of the roadway. Hence, according to characteristics of the V-shaped deviatoric pressure stress distribution, deformation and failure of roadway, more effective support methods need to be developed to account for the roadway under deviatoric pressure from mining disturbance.

6. Conclusions

A roadway under deviatoric pressure caused by mining disturbance is often encountered during working face mining. This paper studied characteristics of deviatoric pressure stress and deformation failure mechanisms of roadways under mining disturbance by the physical model test and the numerical model. Through the comparative analysis of the results, the conclusions can be summarized as follows:

1. The self-developed deviatoric pressure reaction system can better realize deviatoric pressure loading for the physical model.
2. Mining disturbance has an important influence on the

formation of roadway deviatoric pressure. V-shaped deviatoric pressure distribution are easily formed in roadways adjacent to the working face. In the early stage of mining, the deviatoric pressure stress distribution of roadways near the initial mining face is greatly affected by mining, whereas the stress distribution of the roadway near the stopping mining face is less affected by mining. The degree of V-shaped deviatoric pressure in the two roadways increases with the advancing working face.

3. Asymmetric stress distribution caused by deviatoric pressure can easily lead to asymmetric deformation. The mechanism of asymmetric deformation failure in the deviatoric pressured roadway is that first the strength of the surrounding rock is reduced by excavation and mining. Then, working face mining reduces the coal pillar width and causes high pressure stress in the roadway near the initial mining face, which leads to serious deformation and reduces the bearing capacity of the roadway side near the working face, and causes stress to transfer to the other side; meanwhile in the roadway near the stopping mining face, the roadway side near the working face is first affected by mining, which causes high deviatoric pressure and large deformation, but the other side is relatively less affected. Finally, deviatoric pressure stress caused by mining and the strength difference of surrounding rock caused by asynchronous deformation induce asymmetric deformation.

Acknowledgements

This work was supported by the National Natural Science Foundation of China (NSFC) (Grant No. 51574223, No.51704280).

ORCID

Maolin Tian https://orcid.org/0000-0003-2429-1597

References

Coggan J, Gao F, Stead D, Elmo D (2012) Numerical modelling of the effects of weak immediate roof lithology on coal mine roadway stability. *International Journal of Coal Geology* 90-91(1):100-109, DOI: 10.1016/j.coal.2011.11.003

Fu X, Sheng Q, Zhang Y, Chen J (2015) Investigations of the sequential excavation and reinforcement of an underground cavern complex using the discontinuous deformation analysis method. *Tunnelling and Underground Space Technology* 50:79-93, DOI: 10.1016/j.tust.2015.06.010

Gao F, Stead D, Kang HP (2015) Numerical simulation of squeezing failure in a coal mine roadway due to mining-induced stresses. *Rock Mechanics and Rock Engineering* 48(4):1635-1645, DOI: 10.1007/s00603-014-0653-2

He MC (2011) Physical modeling of an underground roadway excavation in geologically 45° inclined rock using infrared thermography. *Engineering Geology* 121(3-4):165-176, DOI: 10.1016/j.enggeo.2010.12.001

He MC, Gong WL, Zhai HM, Zhang HP (2010a) Physical modeling of deep ground excavation in geologically horizontally strata based on infrared thermography. *Tunnelling and Underground Space Technology* 25(4):366-376, DOI: 10.1016/j.tust.2010.01.012

He MC, Jia XN, Gong WL, Lohrasb F (2010b) Physical modeling of an underground roadway excavation in vertically stratified rock using infrared thermography. *International Journal of Rock Mechanics and Mining Sciences* 47(7):1212-1221, DOI: 10.1016/j.ijrmms.2010.06.020

Kang YS, Liu QS, Xi HL (2014) Numerical analysis of THM coupling of a deeply buried roadway passing through composite strata and dense faults in a coal mine. *Bulletin of Engineering Geology and the Environment* 73(1):77-86, DOI: 10.1007/s10064-013-0506-3

Li SC, Wang Q, Wang HT, Jiang B, Wang DC, Zhang B, Li Y, Ruan GQ (2015) Model test study on surrounding rock deformation and failure mechanisms of deep roadways with thick top coal. *Tunnelling and Underground Space Technology* 47:52-63, DOI: 10.1016/j.tust.2014.12.013

Meng QB, Han LJ, Qiao WG, Lin DG, Li H (2016) Numerical simulation research of bolt-grouting supporting mechanism in deep soft rock roadway. *Journal of Mining and Safety Engineering* 33(1):27-34, DOI: 10.13545/j.cnki.jmse.2016.01.005 (in Chinese)

Shen BT (2014) Coal mine roadway stability in soft rock: A case study. *Rock Mechanics and Rock Engineering* 47(6):2225-2238, DOI: 10.1007/s00603-013-0528-y

Sterpi D, Cividini A (2004) A physical and numerical investigation on the stability of shallow tunnels in strain softening media. *Rock Mechanics and Rock Engineering* 37(4):277-298, DOI: 10.1007/s00603-003-0021-0

Sun XM, Chen F, He MC, Gong WL, Xu HC, Lu H (2017) Physical modeling of floor heave for the deep-buried roadway excavated in ten degree inclined strata using infrared thermal imaging technology. *Tunnelling and Underground Space Technology* 63:228-243, DOI: 10.1016/j.tust.2016.12.018

Sun XM, Chen F, Miao CY, Song P, Li G, Zhao CW, Xia X (2018) Physical modeling of deformation failure mechanism of surrounding rocks for the deep-buried tunnel in soft rock strata during the excavation. *Tunnelling and Underground Space Technology* 74:247-261, DOI: 10.1016/j.tust.2018.01.022

Sun J, Wang LG, Zhao GM (2019) Stress distribution and failure characteristics for workface floor of a tilted coal seam. *KSCE Journal of Civil Engineering* 23(9):3793-3806, DOI: 10.1007/s12205-019-0786-7

Sun XM, Zhang GF, Cai F, Yu SB (2009) Asymmetric deformation mechanism within inclined rock strata induced by excavation in deep roadway and its controlling countermeasures. *Chinese Journal of Rock Mechanics and Engineering* 28(6):1137-1143 (in Chinese)

Tian ML, Han LJ, Meng QB, Jin YH, Meng LD (2019) In situ investigation of the excavation-loose zone in surrounding rocks from mining complex coal seams. *Journal of Applied Geophysics* 168:90-100, DOI: 10.1016/j.jappgeo.2019.06.008

Wang YC, Jing HW, Su HJ, Xie JY (2017) Effect of a fault fracture zone on the stability of tunnel-surrounding rock. *International Journal of Geomechanics* 17(6):04016135, DOI: 10.1061/(ASCE)GM.1943-5622.0000837

Xiao TQ, Li HZ, Zhi GH (2014) Experimental study on similar simulation for surrounding rock stability of deep roadway with thick top coal. *Journal of China Coal Society* 39(6):1016-1022, DOI: 10.13225/j.cnki.jccs.2013.1065 (in Chinese)

Yan H, He FL, Wang SG (2014) Safety control and evaluation of roadway with super-large cross-section and soft-weak thick coal

roof. *Chinese Journal of Rock Mechanics and Engineering* 33(5):1014-1023, DOI: 10.13722/j.cnki.jrme.2014.05.017 (in Chinese)

Yang SQ, Chen M, Fang G, Wang YC, Meng B, Li YH, Jing HW (2018) Physical experiment and numerical modelling of tunnel excavation in slanted upper-soft and lower-hard strata. *Tunnelling and Underground Space Technology* 82:248-264, DOI: 10.1016/j.tust.2018.08.049

Yang SQ, Chen M, Jing HW, Chen KF, Meng B (2017) A case study on large deformation failure mechanism of deep soft rock roadway in Xin'An coal mine, China. *Engineering Geology* 217:89-101, DOI: 10.1016/j.enggeo.2016.12.012

Yang XX, Kulatilake PHSW, Jing HW, Yang SQ (2015) Numerical simulation of a jointed rock block mechanical behavior adjacent to an underground excavation and comparison with physical model test results. *Tunnelling and Underground Space Technology* 50:129-142, DOI: 10.1016/j.tust.2015.07.006

Zhang GC, He FL (2016) Asymmetric failure and control measures of large cross-section entry roof with strong mining disturbance and fully-mechanized caving mining. *Chinese Journal of Rock Mechanics and Engineering* 35(4):806-818, DOI: 10.13722/j.cnki.jrme.2015.0917 (in Chinese)

Zhang QB, He L, Zhu WS (2016) Displacement measurement techniques and numerical verification in 3D geomechanical model tests of an underground cavern group. *Tunnelling and Underground Space Technology* 56:54-64, DOI: 10.1016/j.tust.2016.01.029

Zhu WS, Li Y, Li SC, Wang SG, Zhang QB (2011) Quasi-three dimensional physical model tests on a cavern complex under high in-situ stresses. *International Journal of Rock Mechanics and Mining Sciences* 48(2):199-209, DOI: 10.1016/j.ijrmms.2010.11.008

Zhu WS, Zhang QB, Zhu HH, Li Y, Yin JH, Li SC, Sun LF, Zhang L (2010) Large-scale geomechanical model testing of an underground cavern group in a true three-dimensional (3-D) stress state. *Canadian Geotechnical Journal* 47(9):935-946, DOI: 10.1139/T10-006